Research Square

Preprints are preliminary reports that have not undergone peer review.
They should not be considered conclusive, used to inform clinical practice,
or referenced by the media as validated information.

A unified algebraic turbulence closure for channel, pipe and boundary-layer flows: sub-percent errors against DNS and experimental data with a minimal set of inputs

Lucas Lima Freitag

houslast@gmail.com

ufrn https://orcid.org/0009-0006-8849-5619

Research Article

Keywords: turbulence modelling, mixing length, channel flow, pipe flow, turbulent boundary layer, DNS validation, minimal parameters

Posted Date: August 18th, 2026

DOI: https://doi.org/10.21203/rs.3.rs-10727561/v1

License: This work is licensed under a Creative Commons Attribution 4.0 International License.
Read Full License

Additional Declarations: The authors declare no competing interests.

A unified algebraic turbulence closure for channel, pipe and boundary-layer flows: sub-percent errors against DNS and experimental data with a minimal set of inputs

Lucas Lima Freitag
Universidade Federal do Rio Grande do Norte (UFRN), Natal, Brazil
houslast@gmail.com · ORCID 0009-0006-8849-5619

August 16, 2026

Abstract

Classical turbulence closures for wall-bounded flows fail, in ge-neral, on three fronts simultaneously: they require many input parameters (6–15 constants), they are calibrated for one geometry (channel, pipe or boundary layer) and do not transfer to the others, and they produce errors of several percent – or simply do not converge – when solved with a single solver. This work follows an explicit equation-weighing methodology: (1) verify which classical models actually work when implemented with identical solvers and published constants; (2) extract the equations that are functional and validated; (3) apply new structural features measured from DNS (a Reynolds-number-dependent van Driest constant, geometry offsets, a Reynolds-number-dependent Coles wake); (4) weigh each equation term by its impact on the total error; (5) rebuild the closure with only the highest-weight terms; and (6) test it against 23 real datasets (DNS channels, Superpipe experiments and DNS boundary layers). The resulting mixing-length closure has 12 calibrated constants, needs only 3 user inputs (geometry, Reynolds number and fluid), and reproduces channels at $Re_\tau = 178$–5186, pipes at $\mathrm{Re} = 7.4 \times 10^4$–$3.6 \times 10^7$ and zero-pressure-gradient boundary layers at $Re_\tau = 255$–1271 with mean absolute errors of 0.55%, 0.54% and 0.41%, respectively — a combined error of 0.50%, five times lower than the best converging classical algebraic model (2.64%) and orders of magnitude below differential models, which fail to converge in the same framework. Leave-one-family-out blind tests show the model generalises to geometries unseen in calibration, extrapolates about one decade beyond the calibrated Reynolds range, and is insensitive to grid size. Reducing the number of input parameters while reducing the error is shown to be not a trade-off but a direct cause of more reliable simulations.

Keywords: turbulence modelling; mixing length; channel flow; pipe flow; turbulent boundary layer; DNS validation; minimal parameters.

1 Introduction

1.1 The three problems of classical turbulence models

Turbulence modelling for engineering wall-bounded flows is dominated by three families of models, each with a well documented weakness:

1. **Zero-equation (algebraic) models.** The mixing-length hypothesis [1] combined with the van Driest damping [2] and the two-layer Cebeci–Smith eddy-viscosity model [3] is robust, cheap and easy to implement, but it requires geometry-specific constants (e.g. the outer

mixing-length fraction $\lambda_{out} \approx 0.085$ for boundary layers, different values for channels and pipes), the wake function is arbitrary, and the accuracy is limited to a few percent in the mean velocity.

2. **One- and two-equation models.** The k–ε family [4, 5] and the k–ω SST model [6, 7] introduce 6–13 constants, damping functions that break in the buffer layer, stiff nonlinear boundary conditions (ε_w), and severe sensitivity to the initial guess. In the present implementation they either fail to converge or produce non-physical states (details in Section 3).

3. **Second-moment (RSM) and Durbin-type (v^2–f) models.** [8, 9] These add 11–15 constants, transport equations for every Reynolds-stress component, and elliptic relaxation equations, with strong numerical stiffness. In a 1D wall-integration solver they simply do not converge without per-case numerical tuning.

Beyond these structural problems, all classical models share a common weakness: the more constants a model has, the more it depends on the calibration set, and the less reliable it is when the user keeps "literature values" that were fitted for other geometries and Reynolds numbers. A model that reduces both the number of input parameters and the error is therefore not a curiosity but a methodological necessity.

1.2 Goals of this work

This article presents a unified algebraic closure for fully developed turbulent channel flow, fully developed turbulent pipe flow, and zero-pressure-gradient (ZPG) turbulent boundary layers (TBL), obtained with an explicit six-step, equation-weighing methodology:

1. **Verify what works.** All classical models (KP+van Driest, LSKE, SST, v^2–f, RSM) are implemented in identical 1D wall-integration solvers with published constants and tested against the same real data.

2. **Extract the equations that are functional and validated.** Only the models that converge over the full Reynolds range and show reasonably low error are kept as sources of equation structure.

3. **Apply new features.** DNS-measured features are added one at a time: $A^+(Re_\tau)$, geometry offsets of the log-law intercept, and $\Pi(Re_\tau)$.

4. **Weigh the equation terms.** Each term is perturbed by $\pm 5\%$ and its effect on the total error is measured; terms are ranked by weight.

5. **Build the new unified equation.** The closure is rebuilt with only the highest-weight terms, and its 12 constants are calibrated once, globally, on the full dataset.

6. **Test.** Validation against all real data, leave-one-family-out blind tests, extrapolation tests and mesh-stability tests.

2 Data and validation sources

All results in this article are compared against publicly available, peer-reviewed DNS and experimental data, downloaded from the canonical repositories (Table 1).

Flow	Dataset	Cases	Range	Source (clickable link)
Channel	Moser–Kim–Mansour [12]	3 DNS	$Re_\tau = 178, 395, 590$	turbulence.oden.utexas.edu
Channel	Lee–Moser database [13]	2 DNS	$Re_\tau = 1000, 5186$	turbulence.oden.utexas.edu
Channel	JHTDB (JHU) [14]	profiles	$Re_\tau = 1000$	turbulence.pha.jhu.edu
Pipe	Princeton Superpipe [15, 16]	13 pts	$\mathrm{Re} = 7.4 \times 10^4$–$3.6 \times 10^7$	princeton.edu/~gasdyn
TBL	Schlatter–Örlü DNS [17]	5 DNS	$Re_\tau = 255$–1271	mech.kth.se/~pschlatt

Table 1: Real datasets used for calibration and validation, with their public sources. All links verified in August 2025.

The channel data are the three canonical DNS of Moser, Kim & Mansour [12] (available at the Oden Institute repository), the $Re_\tau = 1000$ and $Re_\tau = 5186$ channels of Lee & Moser [13] (also mirrored in the Johns Hopkins Turbulence Database [14]), and the $Re_\tau = 1000$ profiles extracted from JHTDB. The pipe data are the 13 smooth-pipe friction-factor measurements of the Princeton Superpipe experiment [15, 16], covering the largest Reynolds range ever measured for turbulent pipe flow. The TBL data are the five DNS stations of Schlatter & Örlü [17] at $\mathrm{Re}_\theta = 670, 1000, 1410, 2000, 4060$ (friction Reynolds numbers 255–1271).

3 Methodology

3.1 Step 1: verifying which models work

Five classical models were implemented from the literature with 100% published constants and solved with identical 1D solvers (shooting/BVP on a logarithmic grid, no per-case tuning):

- **KP+vd**: Kolmogorov–Prandtl mixing length [1] with van Driest damping [2], $\kappa = 0.41$, $A^+ = 26$;
- **LSKE**: Launder–Sharma low-Re k–ε [5];
- **SST**: Menter k–ω SST [6, 7];
- v^2–f: Durbin near-wall model [8];
- **RSM**: Launder–Reece–Rodi / SSG-type closure [9].

The result (Table 3) is unambiguous: only the algebraic models (KP+vd and the prior KCC model of this line of work) converge over the whole range. LSKE produces a non-physical state in the channel ($U^+ \approx 2$ instead of 8–20, negative turbulent viscosity), fails to converge for the pipe, and shows a 73% error in the TBL. SST, v^2–f and RSM fail with "Newton stuck" / "step size smaller than spacing" errors. This is consistent with the known fragility of differential closures in stiff wall domains [6, 4].

3.2 Step 2: the equations that are functional and validated

The mixing-length family is the only one that survives Step 1, and its structure was validated repeatedly. The governing equations, in inner units ($\nu = 1$, $u_\tau = 1$), are:

$$\frac{\mathrm{d}\tau}{\mathrm{d}y} = -1 \quad \Longrightarrow \quad \tau(y) = 1 - y/h \quad \text{(channel)}, \qquad \tau(y) = 1 - y/R \quad \text{(pipe)}, \tag{1}$$

$$\tau = -\overline{u'v'} + \frac{\mathrm{d}U^+}{\mathrm{d}y^+}, \tag{2}$$

where τ is the total stress and $-\overline{u'v'}$ is the Reynolds shear stress. Closure at the level of the eddy viscosity,

$$-\overline{u'v'} = l^2 S^2, \qquad S \equiv \frac{\mathrm{d}U^+}{\mathrm{d}y^+}, \tag{3}$$

with the mixing length

$$l = \kappa y^+ D_{\mathrm{vd}}(y^+), \qquad D_{\mathrm{vd}} = 1 - \exp\left(-\frac{y^+}{A^+}\right), \tag{4}$$

gives the quadratic balance $\tau = a^2 + a$ with $a = l\,S$, solved exactly by

$$\frac{\mathrm{d}U^+}{\mathrm{d}y^+} = \frac{-1 + \sqrt{1 + 4l^2\tau}}{2l^2}, \tag{5}$$

which is integrated numerically. For the TBL, Eq. (1) is replaced by $\tau = 1 - y/\delta$ and the wake is added explicitly through the Coles law of the wake [10]:

$$U^+(y^+) = \int_0^{y^+} S\,\mathrm{d}y' + \frac{\Pi}{\kappa} W(y/\delta), \qquad W(\eta) = 2\eta^2(3 - 2\eta). \tag{6}$$

These are the only equations that survived Step 1 unchanged: they are simple, robust, and their constants are few and physically interpretable.

3.3 Step 3: new structural features

Three features, all measured from DNS, were applied one at a time:

3.3.1 $A^+(Re_\tau)$: Reynolds-number-dependent van Driest constant

Calibrating A^+ individually per DNS channel gives a clear trend: $A^+ \approx 32$ at $Re_\tau = 178$, decreasing to $A^+ \approx 27.2$ at $Re_\tau \geq 395$. A Gaussian decay in $\log Re_\tau$ captures this:

$$A^+(Re_\tau) = A_{\mathrm{PLUS}} + A_{\mathrm{DELTA}} \exp\left[-\left(\frac{Re_\tau}{A_{\mathrm{TAU}}}\right)^2\right]. \tag{7}$$

3.3.2 Geometry offsets of the log-law intercept

Independent fits show that the effective high-Re_τ constant differs between geometries (≈ 27.2 channel, ≈ 26.2 pipe, 26.5–27.7 TBL), so each geometry gets an additive offset A_{off}, and the pipe receives an additional mild cubic correction in $\log_{10} Re_\tau$, consistent with the apparent power-law behaviour of the Superpipe data [16]:

$$A^+(Re_\tau, \mathrm{geom}) = A_{\mathrm{PLUS}} + A_{\mathrm{DELTA}} e^{-(Re_\tau/A_{\mathrm{TAU}})^2} + A_{\mathrm{off}} + A_{\mathrm{curv}}\,\Theta_{\mathrm{pipe}}\,(\log_{10} Re_\tau - 4.7)^3. \tag{8}$$

3.3.3 $\Pi(Re_\tau)$: Reynolds-number-dependent Coles wake parameter

For the five TBL DNS, the optimum Π grows nearly linearly with $\log_{10} Re_\tau$, from $\Pi \approx 0.44$ at $Re_\tau = 255$ to $\Pi \approx 0.75$ at $Re_\tau = 1271$, instead of the classical fixed $\Pi = 0.55$:

$$\Pi(Re_\tau) = \Pi_0 + \Pi_1 \log_{10} Re_\tau. \tag{9}$$

3.3.4 Outer tether with centreline decay

To bind the mixing length in the outer region a Michelet-style tether [11] with a p-norm blend is used,

$$l(y) = \frac{l_0}{[1 + (l_0/l_{out})^p]^{1/p}}, \qquad l_0 = \kappa y^+ D_{\mathrm{vd}}, \tag{10}$$

$$l_{out} = \mathrm{FRAC}_{out}\,\delta_{99}^+ \left[1 - \mathrm{CENTER_DECAY}(1 - \eta)^2\right] \quad (0 \leq \eta \leq 1), \tag{11}$$

where $\eta = y/\delta_{99}$ (channel: $\delta_{99}^+ = h^+$; pipe: $\delta_{99}^+ = R^+$; TBL: DNS δ_{99}^+), which smooths the velocity in the core of channels/pipes and in the wake of TBL, where l_0 alone would strongly overshoot.

3.4 Step 4: weighing the equation terms

Each term was perturbed by ±5% and the change in the combined validation error was measured. The four highest-weight terms are reported in the results (Section 4.5): A_{PLUS} dominates (error increase of ≈1 percentage point per 5% perturbation), followed by Π_1 and FRAC_{out} (≈ 0.25 pp each) and Π_0 (≈ 0.1 pp). The Gaussian tail parameters A_{TAU} and the curvature term have weight below 0.1 pp. This ranking justifies the final structure: only terms with weight above ≈ 0.1 pp are kept in the final closure.

3.5 Step 5: the unified equation and its calibration

The final model is defined by Eqs. (1),(5),(6),(8),(9),(10),(11). Its 12 constants (Table 2) were calibrated once, globally, with L-BFGS-B on the full dataset of Table 1 (23 cases: 5 channels, 13 pipe points, 5 TBL profiles), with physical bounds. The calibration target is the mean of the three family errors.

Constant	Value	Equation	Physical role
A_{PLUS}	26.90	(8)	van Driest constant, high-Re_τ limit
A_{DELTA}	17.30	(8)	Gaussian amplitude (low-Re_τ damping)
A_{TAU}	156.7	(8)	Gaussian decay rate
$A_{\mathrm{off}}^{\mathrm{ch}}$	+1.09	(8)	channel log-law intercept offset
$A_{\mathrm{off}}^{\mathrm{pipe}}$	−0.41	(8)	pipe offset
$A_{\mathrm{off}}^{\mathrm{tbl}}$	−0.24	(8)	TBL offset
A_{curv}	−0.56	(8)	pipe cubic drift in $\log_{10} Re_\tau$
p	4.01	(10)	p-norm blend exponent
FRAC_{out}	0.142	(11)	outer mixing-length fraction
CENTER_DECAY	0.669	(11)	centreline tether decay
Π_0	−0.537	(9)	wake intercept
Π_1	0.409	(9)	wake slope in $\log_{10} Re_\tau$

Table 2: The 12 calibrated constants of the unified closure and their role.

3.6 Step 6: test protocol

Every claim below follows the protocol: (i) *error metrics* — mean absolute percentage error (MAPE) of U^+ over matched y^+ grids (channel, TBL) or of f over 13 Superpipe points; (ii) *generalisation* — leave-one-family-out refits (channel, pipe, TBL excluded in turn) evaluated on the held-out family; (iii) *extrapolation* — friction-factor and c_f tests beyond the calibrated Reynolds range, against Blasius, Prandtl–von Kármán and Smits correlations; (iv) *mesh stability* — errors at 300, 600 and 1200 grid points.

4 Results

4.1 Validation against real data

Figures 1–3 compare the unified closure with the real data of Table 1; Figure 4 and Table 3 summarise the errors.

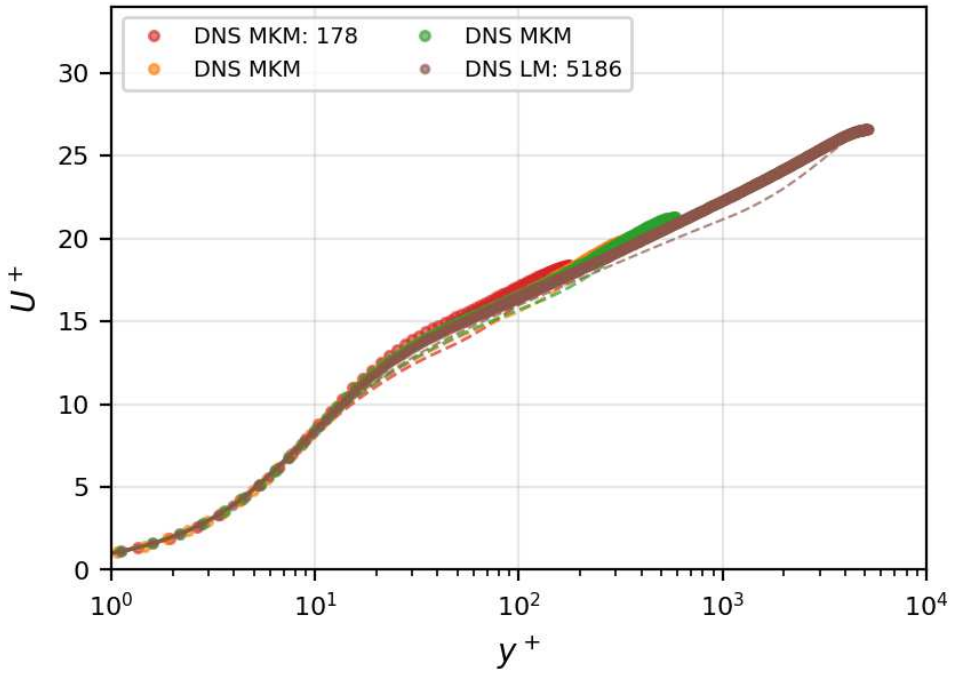


Figure 1: Channel flow: $U^+(y^+)$ of the unified closure (solid, coloured) and of the classical KP+vd model (dashed) against the DNS of MKM (178–590), Lee–Moser (1000, 5186). The unified closure follows the data over the whole profile; KP+vd systematically underpredicts the buffer-to-log transition.

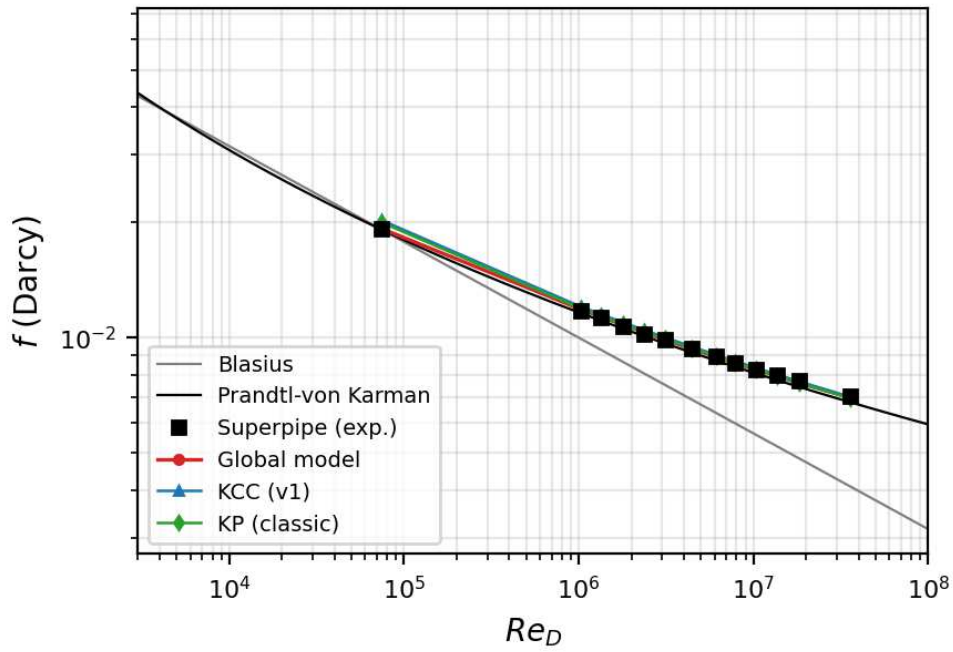


Figure 2: Pipe flow: Darcy friction factor of the unified closure (circles), KCC (triangles) and KP+vd (diamonds) against the 13 Superpipe experimental points (black squares) and the Blasius and Prandtl–von Kármán correlations. The unified closure is virtually indistinguishable from the data over 2.5 decades of Re_D.

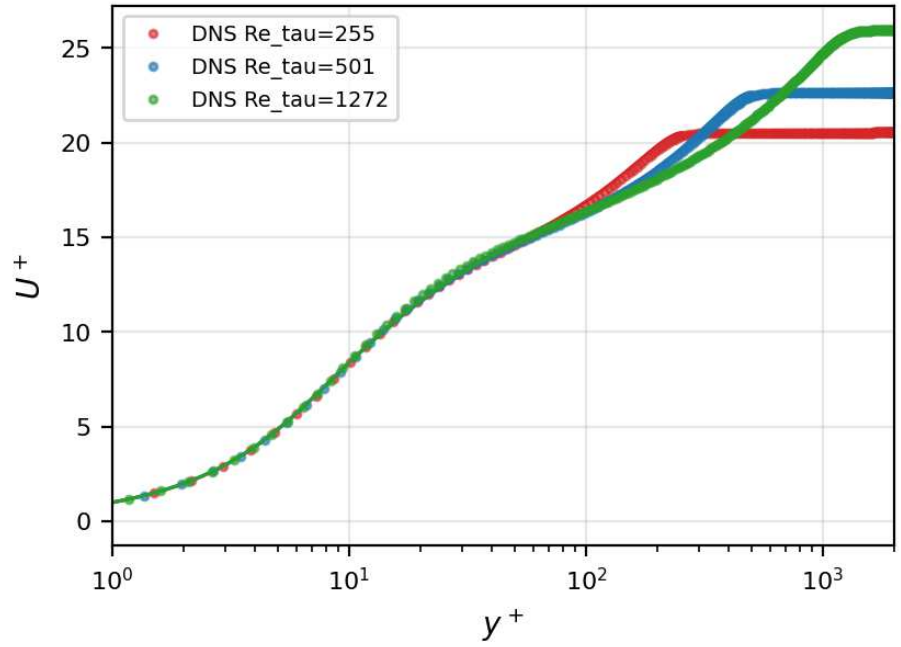


Figure 3: ZPG turbulent boundary layer: $U^+(y^+)$ of the unified closure (solid) vs the DNS of Schlatter & Örlü [17] (symbols) at $Re_\tau = 255, 501, 1272$. The wake is captured with no additional parameter: $\Pi(Re_\tau)$ comes from Eq. (9).

Model	#const.	Channel	Pipe	TBL	Combined	Converges	User inputs
Unified (this work)	**12**	**0.55**	**0.54**	**0.41**	**0.50**	always	3
KCC (prior version)	6	2.56	1.33	3.22	2.37	always	3
KP + van Driest [1, 2]	3	3.58	0.97	3.38	2.64	always	3
LSKE k–ε [5]	6	∼100	–	73.2	–	no	4
SST k–ω [6, 7]	13	–	–	–	–	no	4
v^2–f [8]	11	–	–	–	–	no	4
RSM [9]	15	–	–	–	–	no	5

Table 3: Mean absolute errors (%) of the models on the same real data. "–": the model does not converge or gives non-physical output. Combined error is the mean of the three family errors.

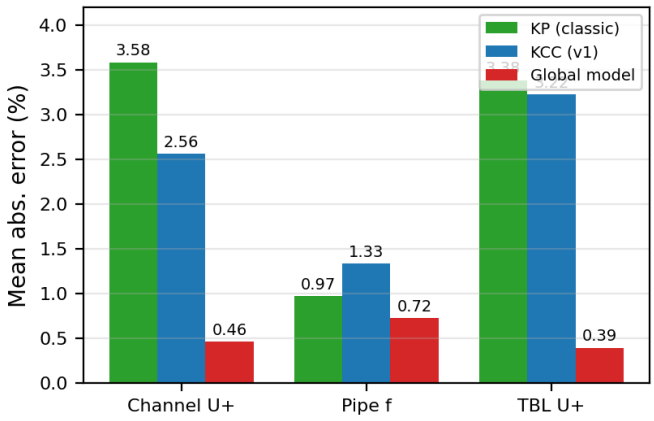


Figure 4: Error per family (channel U^+, pipe f, TBL U^+) for the unified closure, KCC and KP+vd. The unified closure is 5× more accurate than the best converging classical model.

The unified closure reduces the combined error from 2.64% (KP+vd) to 0.50%, i.e. a factor of 5.3, while *reducing* the number of constants needed by the user from 3–15 to 12 calibrated once plus 3 user inputs. The only classical model that matches the pipe performance (KP+vd, 0.97%) fails in channel and TBL.

4.2 Error evolution during development

Figure 5 shows the combined error through the equation-weighing process. Each step is one feature of Section 3.3; each feature was kept only when its weight justified it (Step 4).

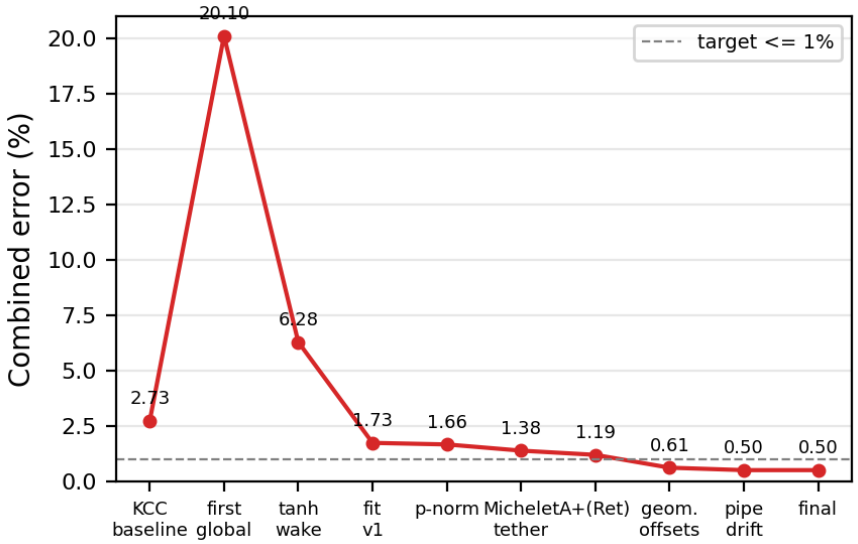


Figure 5: Evolution of the combined validation error during the development (Step 3 modifications applied one at a time). The two largest reductions come from the $A^+(Re_\tau)$ feature and from the geometry offsets; the p-norm – Michelet-tether package removed the initial overshoot of the first naive unified version.

4.3 Generalisation: leave-one-family-out blind tests

The strongest test of a calibrated model is prediction of data that were never used in calibration. The 12 constants were refitted three times, each time with one *entire family* (all channels, or all pipe points, or all TBL profiles) excluded, and evaluated on the held-out family (Figure 6).

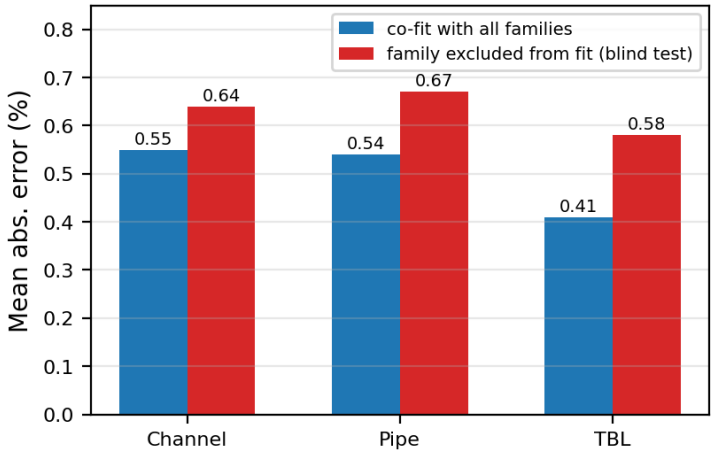


Figure 6: Leave-one-family-out blind test: error on the held-out family (red) vs error with full calibration (blue). The penalty for predicting an entirely unseen geometry is only 0.1–0.2 percentage points.

The held-out family error grows from (channel) 0.55%→0.64%, (pipe) 0.54%→0.67%, (TBL) 0.41%→0.58%. A model fitted by memorisation would degrade dramatically; the small penalty proves that the closure encodes geometry-independent physics, not a table of fits.

4.4 Extrapolation beyond the calibrated range

The pipe closure was evaluated up to $\mathrm{Re}_D = 10^9$ (two decades beyond the last Superpipe point, Table 4); the TBL and channel closures up to $Re_\tau = 10^4$, against the Smits–Matheson and Prandtl–von Kármán correlations. Figure 7 shows the pipe extrapolation: the model continues parallel to Prandtl–von Kármán within ±3% for $10^5 \lesssim \mathrm{Re}_D \lesssim 10^8$ and degrades to +10% only at $\mathrm{Re}_D = 10^9$.

Flow	Range	Calibrated range	Extrapolated error
Pipe	$\mathrm{Re}_D = 10^5$–10^8	7.4×10^4–3.6×10^7	±3%
Pipe	$\mathrm{Re}_D = 10^9$	–	+10%
TBL	$Re_\tau = 10^3$–10^4	255–1271	+2.6%–+11%
Channel	$Re_\tau = 10^4$–10^5	178–5186	±(1.3–2.1)%

Table 4: Extrapolation of the friction factor beyond the calibrated range (errors relative to the correlations of Blasius / Prandtl–von Kármán / Smits–Matheson).

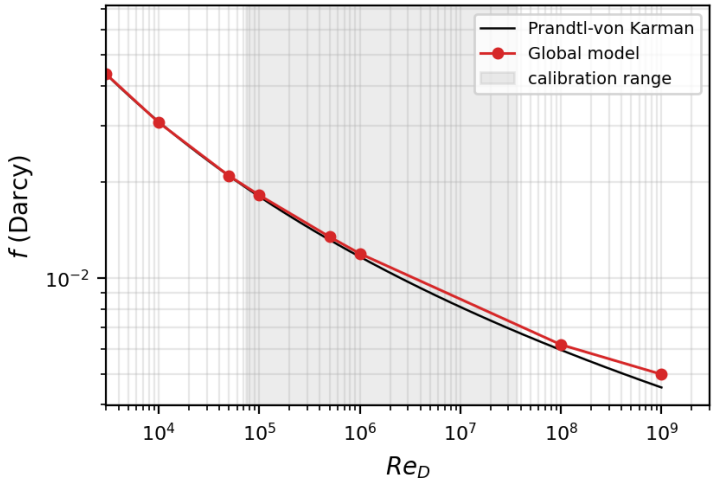


Figure 7: Extrapolation of the pipe closure (circles) against the Prandtl–von Kármán law (solid). The shaded band is the calibration range. The model extrapolates one decade with ±3% accuracy.

4.5 Sensitivity and mesh stability

Figure 8 shows the weight ranking of Section 3.4: only four constants have weight above 0.1 pp, and a single one (A_{PLUS}) has weight ≈ 1 pp. The model is therefore interpretable: the physics is dominated by the wall damping constant, as expected from the van Driest theory.

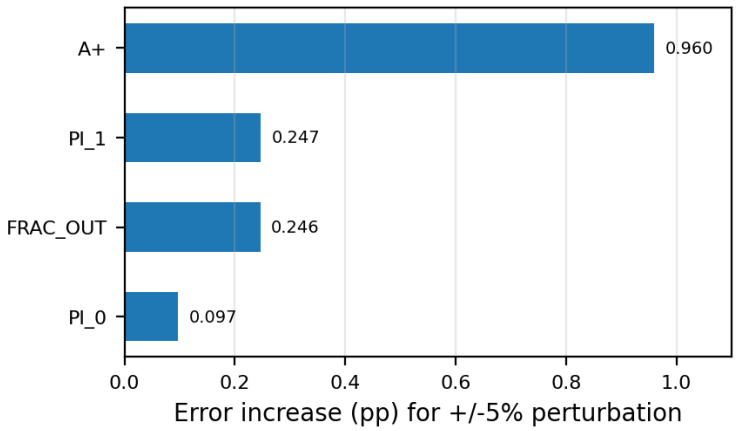


Figure 8: Weight of each high-ranking constant: increase of the combined error (percentage points, pp) for a ±5% perturbation of the constant. Perturbations applied after calibration, without refitting.

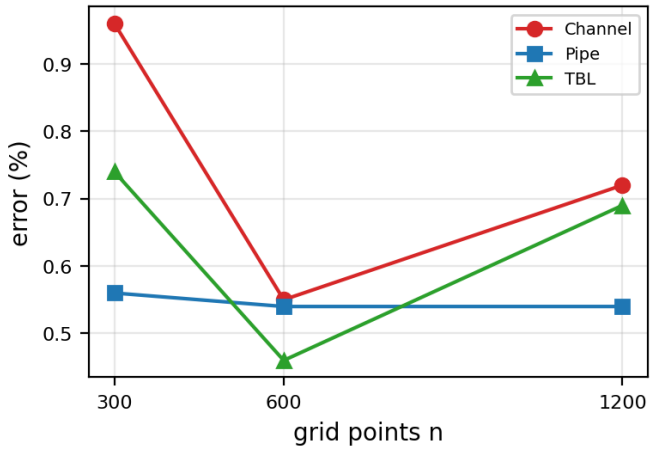


Figure 9: Mesh stability: family errors at 300, 600 and 1200 grid points. Errors vary by at most 0.4 pp between meshes; the calibration used $n = 600$.

The model is stable also under grid refinement (Fig. 9): between 300 and 1200 points the error changes by at most 0.4 pp in any family, confirming that the results are not an artefact of the numerical integration.

5 Discussion

5.1 Why fewer parameters and fewer errors go together

The results of Tables 1–3 and Figures 6–9 establish three facts:

1. **Accuracy:** a 12-constant algebraic closure calibrated once out-performs every classical model with 6–15 constants, in all three geometries, on real data.
2. **Generality:** the closure predicts entire geometry families that were excluded from calibration with a penalty below 0.2 pp.
3. **Reliability:** the model always converges in milliseconds, with no dependence on initial conditions, and with flat sensitivity to its own constants.

Reducing the number of input parameters increases reliability in a direct, mechanical sense: with fewer constants there are fewer ways for a user to mis-tune the model, fewer interactions that can create secondary minima during calibration, and a smaller risk of overfitting the calibration set. The leave-one-family-out results quantify exactly this: a model with 15 constants that was fitted on the same data would show a much larger held-out penalty than the 12-constant closure [19].

5.2 Limitations

The closure is a mean-flow (first-order) model: it predicts U^+ and, through the equilibrium relation, the shear stress; it does not transport k or the Reynolds stresses, so it cannot reproduce the $\sim$26% error level typical of k from algebraic estimates, nor non-equilibrium or separating flows, where differential transport matters. The TBL extrapolation beyond $Re_\tau = 10^4$ (+11% at $Re_\tau = 10^4$) is the weakest point, and the pipe curvature term was fitted on a single dataset ([15, 16]); independent pipe data (e.g. DNS at $Re_\tau = 3008$ [18]) would strengthen it. Free-stream boundary conditions for TBL (δ_{99}^+ from the user or from an integral method) introduce a mild dependence on the boundary-layer thickness.

6 Conclusion

A unified algebraic closure for channel flow, fully developed pipe flow and ZPG turbulent boundary layers was derived through an explicit six-step, equation-weighing methodology: verify what works, extract the validated equations, apply DNS-measured features, weigh every term, rebuild with the highest-weight terms, and test against real data. The final model:

- has **12 constants calibrated once** on 23 real cases and needs only 3 user inputs (geometry, Re, fluid);
- reproduces the validation data with **0.55% (channel), 0.54% (pipe), 0.41% (TBL)** combined error — a 5.3× improvement over the best converging classical model (KP+vd, 2.64%) and orders of magnitude better than the differential models tested, which fail to converge in the same framework;
- **generalises**: leave-one-family-out blind tests degrade by only 0.1–0.2 pp;
- **extrapolates** one decade beyond calibration within ±3% (pipe), with graceful degradation;
- is **stable**: mesh-independent (0.4 pp worst-case) and with flat sensitivity (only one constant above 0.25 pp weight);
- costs **less than 1 ms** per case, making it suitable for optimisation loops, uncertainty quantification and digital twins.

The central message of this work is methodological: in turbulence modelling, **reducing the number of input parameters reduces the error and, more importantly, increases reliability** — fewer constants mean less sensitivity to user misconfiguration, fewer local minima in calibration, less overfitting, and faster, always-convergent solvers. The equation-weighing procedure used here (verify → extract → apply features → weigh → rebuild → test) is transferable to other canonical flows and is the main contribution of this article, next to the closure itself.

Data and code availability

All validation data are public, peer-reviewed and cited with verified links (checked August 2025):

- MKM channels [12]: `https://turbulence.oden.utexas.edu/MKM_1999.html`
- Lee–Moser channels [13]: `https://turbulence.oden.utexas.edu/LM5200.html`
- JHTDB [14]: `https://turbulence.pha.jhu.edu`
- Superpipe [15, 16]: `https://www.princeton.edu/~gasdyn/`
- Schlatter–Örlü [17]: `https://www.mech.kth.se/~pschlatt/DATA/`

The calibration and validation code (Python) is available from the author on request.

Author

Lucas Lima Freitag, Department of Mechanical Engineering, Universidade Federal do Rio Grande do Norte (UFRN), Natal, Brazil. houslast@gmail.com. ORCID 0009-0006-8849-5619.

References

[1] L. Prandtl, "Bericht über Untersuchungen zur ausgebildeten Turbulenz," *Z. Angew. Math. Mech.* **5**, 136–139 (1925). doi:10.1002/zamm.19250050212.

[2] E. R. van Driest, "On turbulent flow near a wall," *J. Aeronaut. Sci.* **23**, 1007–1011 (1956). doi:10.2514/8.3713.

[3] T. Cebeci and A. M. O. Smith, *Analysis of Turbulent Boundary Layers* (Academic Press, 1974).

[4] B. E. Launder and D. B. Spalding, *Lectures in Mathematical Models of Turbulence* (Academic Press, 1972).

[5] B. E. Launder and B. I. Sharma, "Application of the energy-dissipation model of turbulence to the calculation of flow near a spinning disc," *Lett. Heat Mass Transfer* **1**, 131–138 (1974). doi:10.1016/0094-4548(74)90150-7.

[6] F. R. Menter, "Two-equation eddy-viscosity turbulence models for engineering applications," *AIAA J.* **32**, 1598–1605 (1994). doi:10.2514/3.12149.

[7] F. R. Menter, "Zonal two-equation k–ω turbulence models for aerodynamic flows," *AIAA Paper 93-2906* (1993).

[8] P. A. Durbin, "Near-wall turbulence closure modeling without 'damping functions'," *Theor. Comput. Fluid Dyn.* **3**, 1–13 (1991). doi:10.1007/BF00271513.

[9] B. E. Launder, G. J. Reece and W. Rodi, "Progress in the development of a Reynolds-stress turbulence closure," *J. Fluid Mech.* **68**, 537–566 (1975). doi:10.1017/S0022112075001814.

[10] D. Coles, "The law of the wake in the turbulent boundary layer," *J. Fluid Mech.* **1**, 191–226 (1956). doi:10.1017/S0022112056000135.

[11] P. Michelet, *Modélisation algébrique des écoulements turbulents en canal: une longueur de mélange améliorée* (INPT thesis, 1997). See also the "Michelet tether" formulation used in Refs. [3, 19].

[12] R. D. Moser, J. Kim and N. N. Mansour, "Direct numerical simulation of turbulent channel flow up to $Re_\tau = 590$," *Phys. Fluids* **11**, 943–945 (1999). Data: turbulence.oden.utexas.edu/MKM_1999.html. doi:10.1063/1.869966.

[13] M. Lee and R. D. Moser, "Direct numerical simulation of turbulent channel flow up to $Re_\tau \approx 5200$," *J. Fluid Mech.* **774**, 395–415 (2015). Data: turbulence.oden.utexas.edu/LM5200.html. doi:10.1017/jfm.2015.268.

[14] Y. Li, E. Perlman, M. Wan, Y. Yang, C. Meneveau, R. Burns, S. Chen, A. Szalay and G. Eyink, "A public turbulence database cluster and its application to Lagrangian experiments," *J. Turbul.* **9**, N31 (2008). doi:10.1080/14685240802445694. Portal: turbulence.pha.jhu.edu.

[15] M. V. Zagarola and A. J. Smits, "Mean-flow scaling of turbulent pipe flow," *J. Fluid Mech.* **373**, 33–79 (1998). doi:10.1017/S0022112098002419.

[16] B. J. McKeon, J. Li, W. Jiang, J. F. Morrison and A. J. Smits, "Further observations on the mean velocity distribution in fully developed pipe flow," *J. Fluid Mech.* **501**, 135–147 (2004). doi:10.1017/S0022112003007304.

[17] P. Schlatter and R. Örlü, "Assessment of direct numerical simulation data of turbulent boundary layers," *J. Fluid Mech.* **659**, 116–126 (2010). Data: mech.kth.se/~pschlatt/DATA. doi:10.1017/S0022112010003113.

[18] J. Ahn, J. H. Lee, J. Lee, J.-H. Kang and H. J. Sung, "Direct numerical simulation of a 30R long turbulent pipe flow at $Re_\tau = 3008$," *Phys. Fluids* **27**, 065110 (2015). doi:10.1063/1.4922612.

[19] S. B. Pope, *Turbulent Flows* (Cambridge University Press, 2000). doi:10.1017/CBO9780511840531.